Laboratory and Numerical Evaluation of Borehole Methods for Subsurface Horizontal Flow Characterization

William H. Pedler and Richard Jepsen

Sandia National Laboratories

Laboratory and Numerical Evaluation
Of Borehole Methods for Subsurface
Horizontal Flow Characterization

Richard Jepsen
Carlsbad Programs Group
Sandia National Laboratories
4100 National Parks
Carlsbad, NM 88220

William H. Pedler
Radon Abatement Systems, Inc.
Integrated Subsurface Evaluation
311 Rock Avenue
Golden, Colorado   80401

Abstract

The requirement to accurately measure subsurface groundwater flow at contaminated sites, as part of a time and cost effective remediation program, has spawned a variety of flow evaluation technologies. Validation of the accuracy and knowledge regarding the limitations of these technologies are critical for data quality and application confidence. Leading the way in the effort to validate and better understand these methodologies, the US Army Environmental Center has funded a multi-year program to compare and evaluate all viable horizontal flow measurement technologies. This multi-year program has included a field comparison phase, an application of selected methods as part of an integrated site characterization program phase, and most recently, a laboratory and numerical simulator phase.

As part of this most recent phase, numerical modeling predictions and laboratory measurements were made in a simulated fracture borehole set-up within a controlled flow simulator. The scanning colloidal borescope flowmeter (SCBFM) and advanced hydrophysical

logging (NxHpL™) tool were used to measure velocities and flow rate in a simulated fractured borehole in the flow simulator. Particle tracking and mass flux measurements were observed and recorded under a range of flow conditions in the simulator. Numerical models were developed to aid in the design of the flow simulator and predict the flow conditions inside the borehole.

Results demonstrated that the flow simulator allowed for predictable, easily controlled, and stable flow rates both inside and outside the well. The measurement tools agreed well with each other over a wide range of flow conditions. The model results demonstrate that the Scanning Colloidal Borescope did not interfere with the flow in the borehole in any of the tests. The model is capable of predicting flow conditions and agreed well with the measurements and observations in the flow simulator and borehole. Both laboratory and model results showed a lower limit of fracture velocity in which inflow occurs, but horizontal flow does not establish itself in the center of the borehole. In addition, both laboratory and model results showed circulation cells in the borehole above and below the fracture horizon. The length of the interval over which the circulating cells occurred was much larger than the interval of actual horizontal flow. These results suggest that for the simple fracture geometry simulated in this study, horizontal flow can be predictable and measurable, and that this flow is representative of the larger, near-field flow system. Additional numerical refinements and laboratory simulations of more robust, life-like fracture geometries should be considered.

The preliminary conclusions of this work suggest the following: 1) horizontal flow in the fractured medium which is representative of the near-field flow conditions can be established in a wellbore; 2) this horizontal flow can be accurately measured and numerically predicted; 3) the establishment of directionally quantifiable horizontal flow is dependent on four parameters: borehole diameter, structure, permeability and the hydraulic gradient of the flowing feature; and, 4) by measuring three of these four parameters, the fourth parameter can be numerically derived through computer simulations.

Acknowledgements

This page left intentionally blank.

CONTENTS

LIST OF FIGURES

LIST OF TABLES

1.0 Introduction

This study is the third phase of a multi-year evaluation and comparison of horizontal flow measurements in the fractured and karst setting. The first phase involved a comparison of four different techniques in two karst settings with the results summarized by Wilson, et al., 1999. The conclusions of this report were that the particle tracking type measurements (fixed focal point colloidal borescope and acoustic Doppler flow meter) had a wide range of results, were not comparable with each other, not repeatable and varied considerably over short vertical distances. The hydrophysical logging (HPL) method continued to display its superior capability in identifying horizontal flow intervals and had comparable velocity results with the KV heat dilution device. Based on these results, and the discovery of the Scanning Colloidal borescope developed at Lawrence Livermore National Laboratory, Phase II of this study was a focused field application of the HPL and SCBFM at Camp Crowder in Missouri. Unlike the fixed focal point colloidal borescope deployed during phase one, the SCBFM can scan through a 500mm interval. This was the first application of the SCBFM in the fractured karst environment and proved very enlightening. By using HPL to locate the horizontal flow areas and then deploying the SCBFM, it was discovered that the horizontal flowing intervals were very thin (4-5cm) and of high velocity and consistent direction. Another important discovery was the identification of swirling intervals above and below the identified fast pathway. These swirling cells were highly variable in direction and velocity, and sometimes consistently flowing at 180 degrees from the identified fast pathway. These discoveries put the Phase I data into context for the first time. The importance of resolving the flow over an interval, as opposed to a fixed point, becomes paramount to accurately evaluating horizontal flow in a borehole in the fractured regime.

After the success of Phase II, when the combined approach of HPL and the SCBFM was determined to accurately find and characterize horizontally flowing features, the question arose regarding how representative horizontal flow in a wellbore was to the surrounding fractured system. This is a complex issue and begs the longstanding question; "How representative is *anything* in the borehole to the system as a whole?"

As such, this phase of the study looked at a simple fracture, set in a known and controllable horizontal flowing environment, to simulate flow behavior in both a numerical and laboratory setting.

In addition, the effect of the scanning borescope itself on the flow field was modeled for several flow conditions and geometries.

2.0 Laboratory Simulator Experimental Set-up

2.1 Laboratory Simulator

Based on the work of Drost (1967) and others, a laboratory scale horizontal flow chamber was constructed (Figure 2.1). The objective of this chamber was to create a stable horizontal flowing condition in a porous medium. The dimensions of the simulator were 3 ft wide by 4 ft deep by 7 ft long. Two six inch reservoirs were located at each end such that the overall length was 8 feet, and such that water could be circulated in both directions through the chamber at a known flow rate with an associated observable horizontal gradient.

Once the flow simulator was constructed and filled with sand, the actual permeability of the flow simulator was calculated to be 2.1E-9 m^2. The sand was a well-rounded, well-sorted coarse sand (8/16) with a bulk porosity of 34.5 %. The permeability for this sand type is reported to be between 1.0E-9 and 1.0E-10 m^2 (Bear et. al., 1968).   Actual calculation of permeability was performed by pumping at 9.0 gallons per minute (gpm) across the tank and generating a corresponding 0.074 m head difference. The tank was filled to 0.91 m prior to pumping. Using Darcy's Law, where *Sd* is specific discharge or Darcy velocity:

$$Sd = V = \frac{K\Delta h}{L}$$
(2.1)

Since the flow simulator tank is 0.91 m wide and 2.2 m long, V = 6.92E-4m/s and L= 2.2m. Therefore, for Δh of 0.074 m, the hydraulic conductivity, K, is 2.06E-2 m/s. Hydraulic conductivity was also calculated for a second pumping rate of 4.0 gpm with resulting K = 1.96E-2 m/s.

The following relationship was used to calculate permeability:

$$K = \frac{kg}{v}$$
(2.2)

Where k is the permeability, g is the gravitational constant, 9.81 m/s^2 and ν is the kinematic viscosity of water, 1E-6m^2/s. Using 0.0206 m/s for the hydraulic conductivity gives 2.1E-9 m^2 for the permeability.

Figure 2.1. Laboratory simulator for horizontal flow. Note the reservoirs at both ends and acrylic "fractured borehole" in center.

2.2 Well Simulation

To simulate a simple horizontal fracture regime, two slots were cut in a 4-inch acrylic tube that was installed in the center of the flow chamber. These slots were 1.5 millimeter wide and diametrically opposed to each other with a 90 degree cut out on each side. The openings were oriented perpendicular to the long axis (flowing direction) of the simulator. This was designed to simulate a simple horizontal fracture with a partial (50%) opening. Please refer to Figure 2.2.

Four re-circulating rates were employed during horizontal flowing simulations and corresponded to similar flow rates used for the numerical modeling. The scanning colloidal borescope and the advanced hydrophysical tool were deployed during these pumping rates.
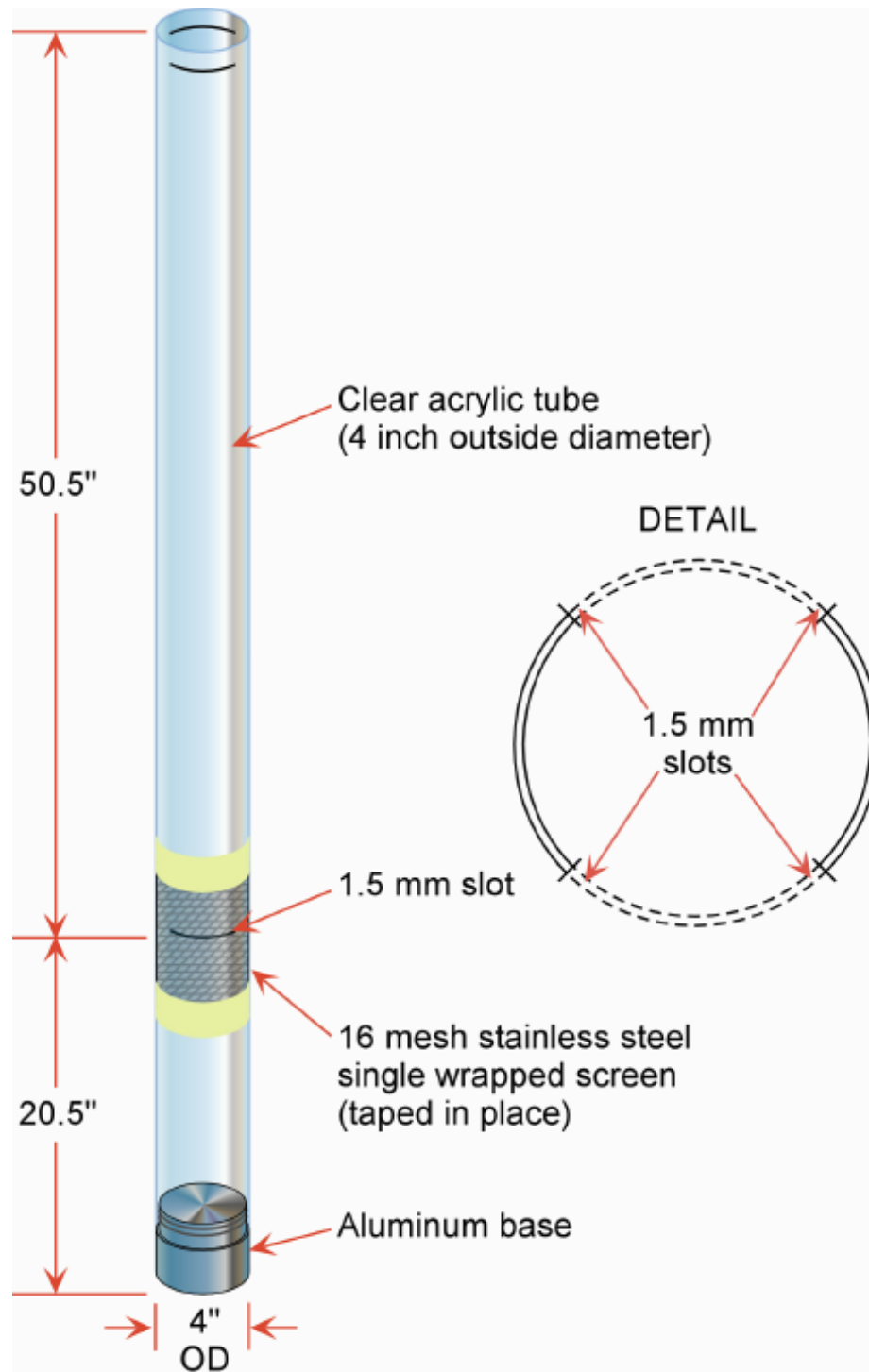
Figure 2.2. Schematic of fracture used in study.

2.3 Scanning Colloidal Borescope Flow Meter (SCBFM)

        The scanning colloidal borescope flow meter is used to evaluate horizontal groundwater flow direction and velocity. The SCBFM employs a CCD, magnetometer, light source and a remotely controlled, variable focal point lens mechanism to track colloidal sized particles (1-5 microns). Please refer to to Figure 2.3.
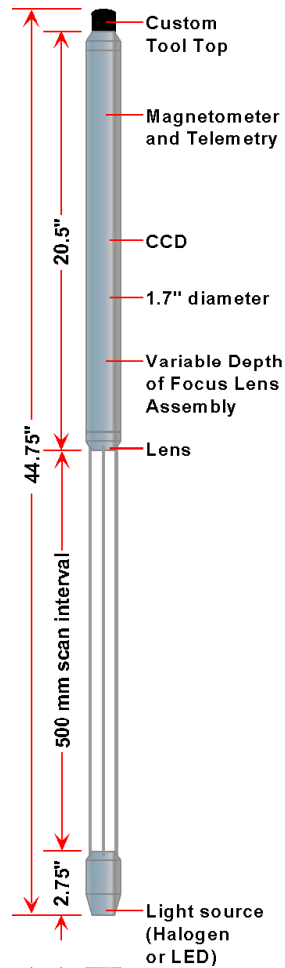
Figure 2.3. Schematic of Scanning Colloidal Borescope Flow Meter.

        Naturally occurring colloids move advectively with the native groundwater system. By recording the output of the CCD and using advanced particle-tracking computer software, the compass direction and advective velocity of horizontal groundwater flow in a well can be evaluated. The scanning feature allows a 500mm interval to be evaluated, as opposed to a single

fixed point. This scanning feature allows for a three dimensional evaluation such that swirling, non-representative flow cells can be identified and more importantly, "fast pathways" can be detected and characterized. The SCBFM was originally conceived and developed by Lawrence Livermore National Laboratory (LLNL).

2.4 Hydrophysical Logging

RAS's proprietary advanced hydrophysical logging method (NxHpL™) (Pedler and Urish, 1988, Pedler et.al. 1990, 1992, 1992a, and others, see reference section) is based on replacing the fluid column in a wellbore with deionized water and then profiling the induced changes in the electrical properties of the emplaced fluid column. The electrical properties are profiled as a function of time with a proprietary, high-resolution fluid electrical conductivity (FEC) and temperature tool. RAS's multi-sensor tool employs up to eight FEC and temperature sensors in a variety of configurations. For the project in the horizontal flow simulator, RAS employed a four-sensor array, with the sensors vertically spaced six inches apart and rotated horizontally at ninety degrees. Please refer to Figure 2.4 for details.
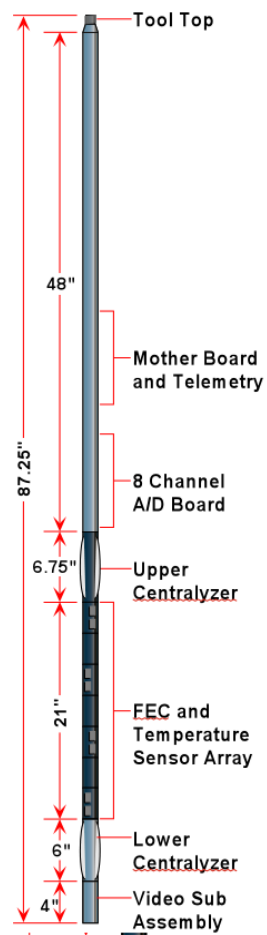
Figure 2.4. Schematic of the RAS multi-sensor HPL tool with optional video subassembly.

2.5 Test Protocol

The following briefly summarizes the test protocol:

1) Measure and record background water level measurements at datum points.

2) Start pumping at target pumping rate. Measure and record instantaneous flow rate, total gallons, and depth to water at each datum point.

3) Monitor the system until a steady state condition is observed.

4) Start tool data collection and record data. In the case of hydrophysical logging, flush wellbore with deionized water, then insert tool and take measurements.

3.0 Results of SCBFM and Hydrophysical Logging

3.1 Scanning Colloidal Borescope

The SCBFM was deployed during 0, 0.4, 1.0, and 2.5 gpm flow tests. The SCBFM was also applied during the 4.0 gpm flow test, but the in-hole velocity, estimated at over 5000μm/sec, exceeded the capability of SCBFM's present software. This is a software limitation and not an inherent limitation. An example of the recorded data is given below in Figure 3.1.
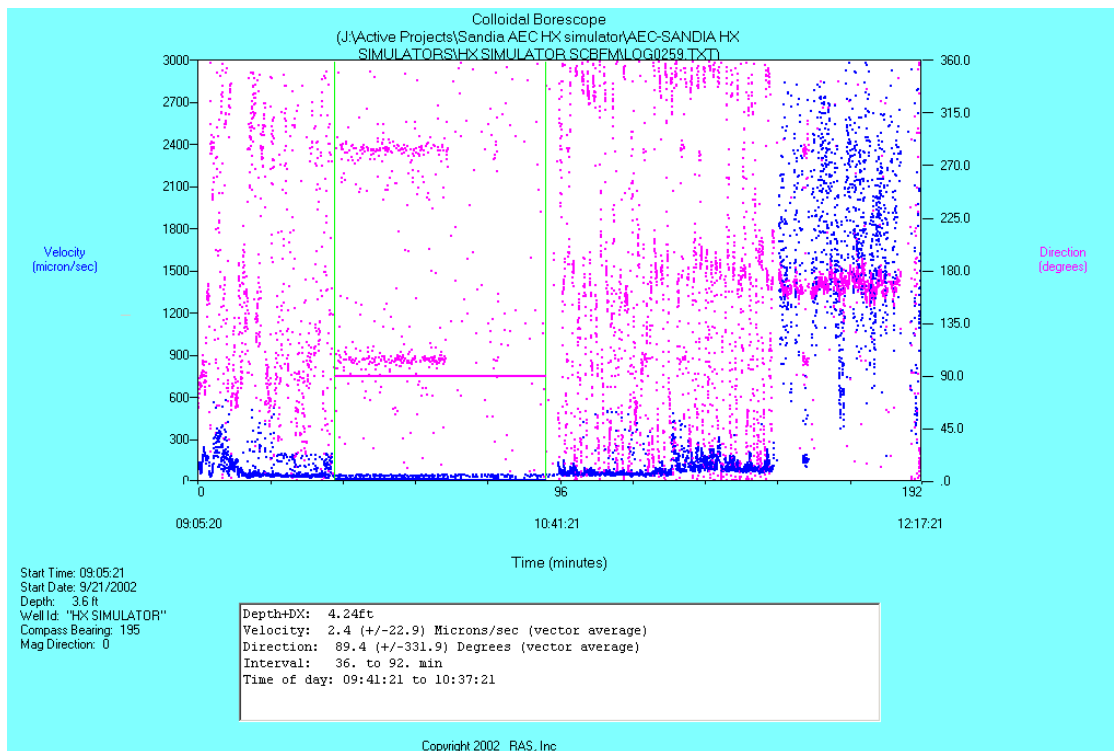
Figure 3.1. Example of SCBFM data, vertical green bars indicate time over which average velocity and direction was calculated. Velocity is plotted in blue, with the axis on the left. Direction is plotted in magenta, with the axis on the right. These results are presented in the center box. Average period presented corresponds to a no pumping and no flow condition.

3.2 Hydrophysical Logging

Hydrophysical logging was conducted at flow rates similar to those for the SCBFM and under similar, and previously described, procedures.

An example of the hydrophysical logging results and analysis is given in Figure 3.2 below.
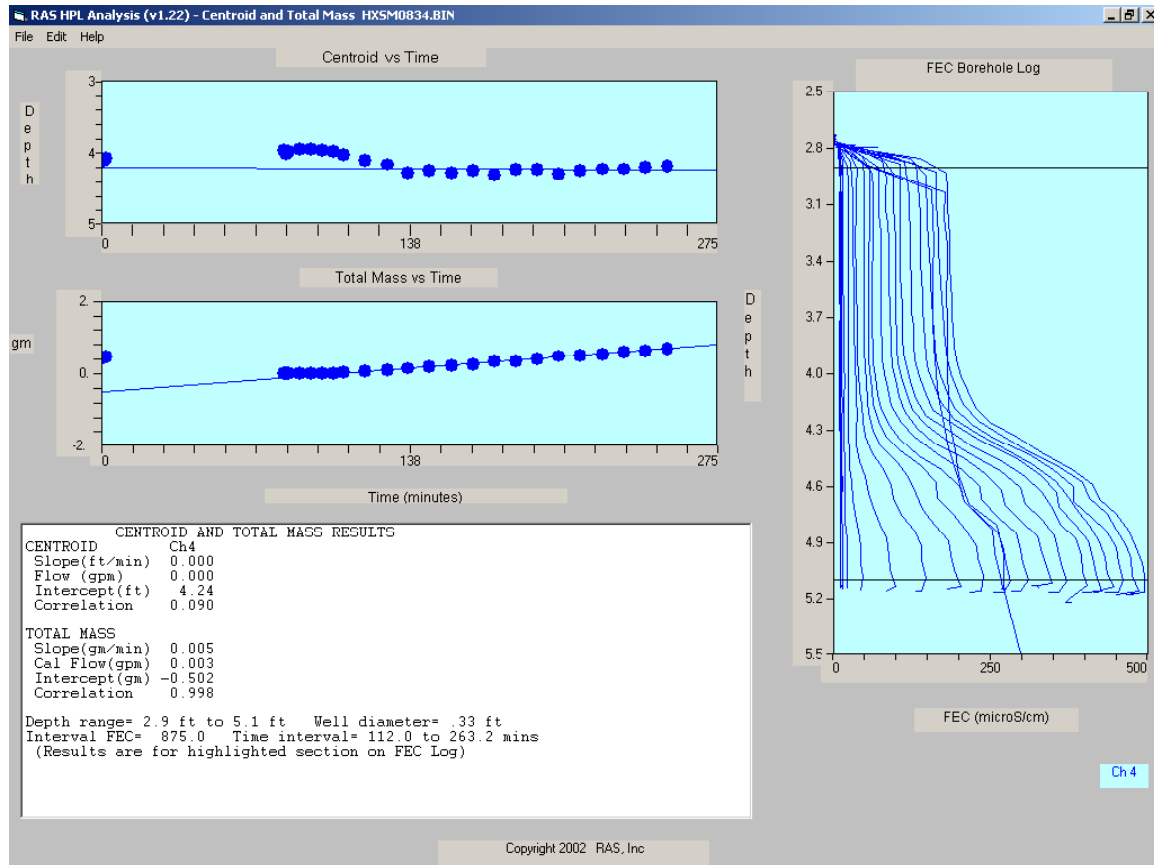
Figure 3.2. Results of HPL in HX simulator, pumping rate of ~0.4 gpm with 0.02'/7' = 2.86e-3 feet/feet or 0.28' in 100' horizontal hydraulic gradient.

A summary of the average flow velocity measured by the SCBFM and NxHpL™ results is presented below in Table 3.2

Table 3.2. Summary of Hydrophysical Logging and SCBFM Results.

| Pumping Rate (gpm) | Hydrophysical Logging | | | | SCBFM |
| | Integral Analysis | | Dilution Analysis | | |
	Flowrate (gpm)[1]	Inlet Fracture Velocity (microns/sec)	Flow velocity (ft/day)[2]	Inlet Fracture Velocity (microns/sec)[3]	Velocity at borehole center (microns/ sec)
0.0					2
0.4	0.003	1,590	2.66	9.50	55
1.0					110
1.3	0.005	2,647	6.04	21.6	
2.5	0.008	4,235	7.47	26.7	1600
4.0	0.010	5,294	13.04	46.6	

4.0 Numerical Simulator – Computer Modeling

Modeling studies were performed for all geometries and flow conditions used in the laboratory flow simulator experiments. The numerical models were generated using Adaptive Research's Stormflow computational fluid dynamic software to simulate flow fields subject to specified initial and boundary conditions. The software was run on a standard desktop computer with an Intel 2.2 GHz processor running Windows 2000. The availability of this cost effective computing platform allowed for this level of numerical simulations for the first time.

Numerical computations were done for three basic purposes: 1) to determine appropriate design for flow simulator dimensions; 2) to determine the inlet velocity at the fracture into the open well from the porous media; 3) to determine the flow conditions inside the well with the borescope; and, 4) to evaluate the effect the SCBFM had on the horizontal flow.

---

[1] Flowrate based on integral method of analysis (Lowe, et al, ..)

[2] Flow velocity based on dilution analysis (Drost, et al, 1967)

[3] Calculated on 3.57 microns/sec = 1 ft/day

4.1 Laboratory Flow Simulator

Prior to construction, the RAS flow simulator was modeled to investigate the effects of the well and the sidewalls on the flow field. This was done using a porous media in the flow simulator with a permeability of 2.1E-9 m^2. Figure 4.1 shows the geometry and grid configuration with a 4-inch well in the simulator.
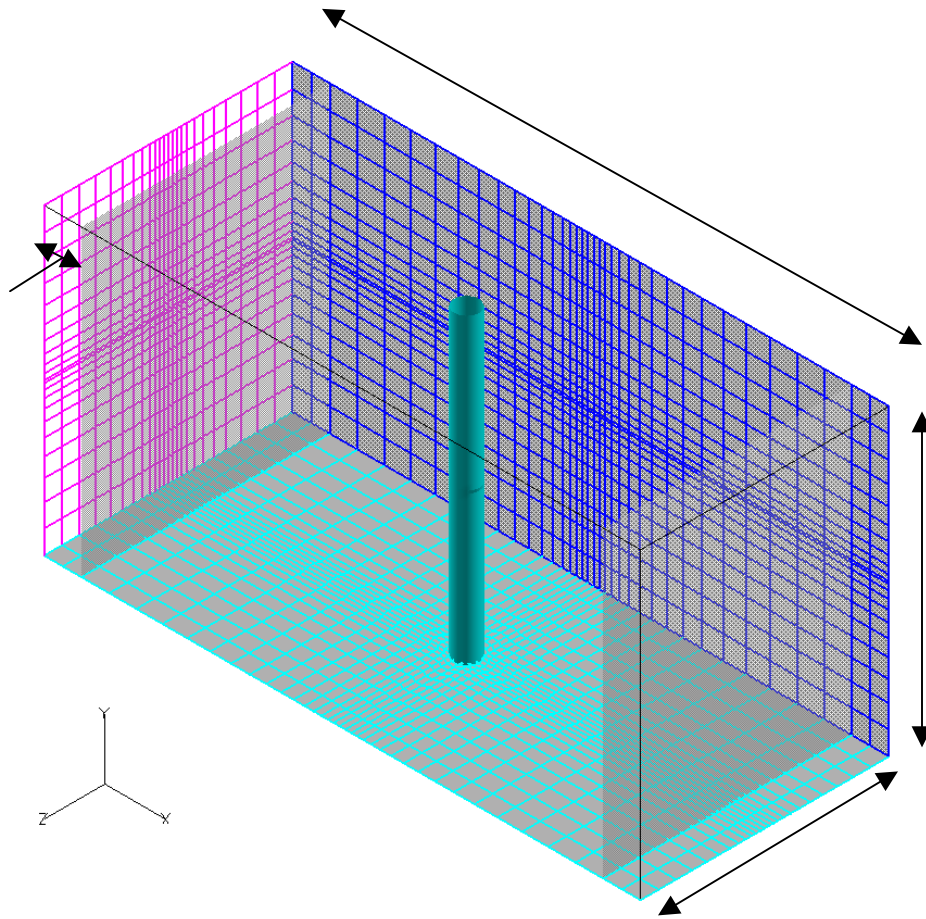
Figure 4.1. Isometric view of geometry and grid cells in the flow simulator with a 4-inch well.

The grid spacing near the well was increased to gain detail of the flow field near the well. Results of these modeling tests demonstrated that the tank was designed with the appropriate length and width.

Figure 4.2 shows the results of the pressure field across the simulator for a 3.25 cm head difference (4.0 gpm flow rate). The change in pressure was calculated to be 290 Pa. This is very close to the 320 Pa calculated using ρgΔh for the change in pressure.
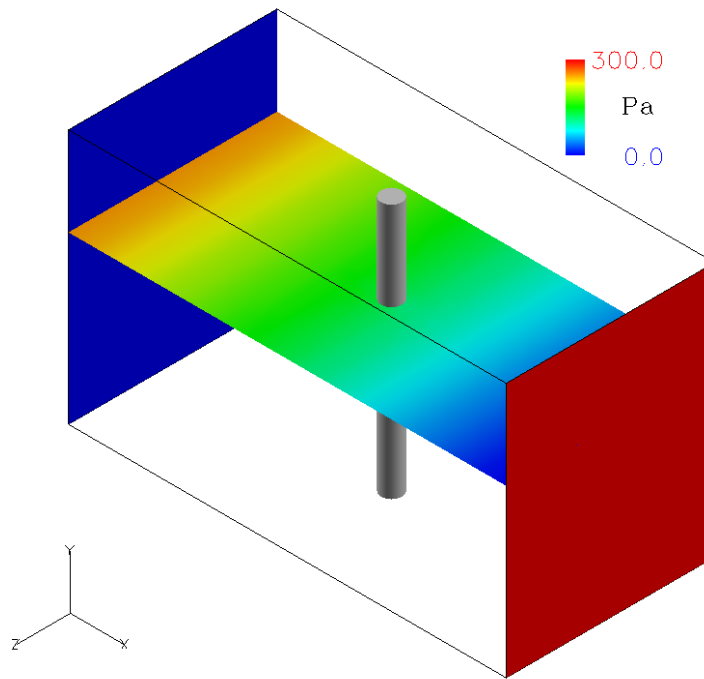
Figure 4.2. Isometric view of the pressure field (Pa) in the flow simulator around a 4-inch well with a 4.0 gpm pumping rate. Flow is from left to right with the inlet in blue and the outlet in red.

Figure 4.3 shows the results for the velocity field in the simulator for a pumping rate of 4.0 gpm across the tank. Figure 4.4 shows a close-up near the well using contours for the velocity. The results demonstrate that the effects on the flow field due to the well obstruction and sidewalls are very local. The effects of the well obstruction are not seen beyond 15 cm of the well (Figure 4.4). Thus, the flow simulator has sufficient dimensions for the tests to be performed. In addition, a smaller model geometry and grid size can be used to determine the inlet velocity into the fractured well from the flow conditions in the flow simulator. These issues are discussed in more detail in the following section.
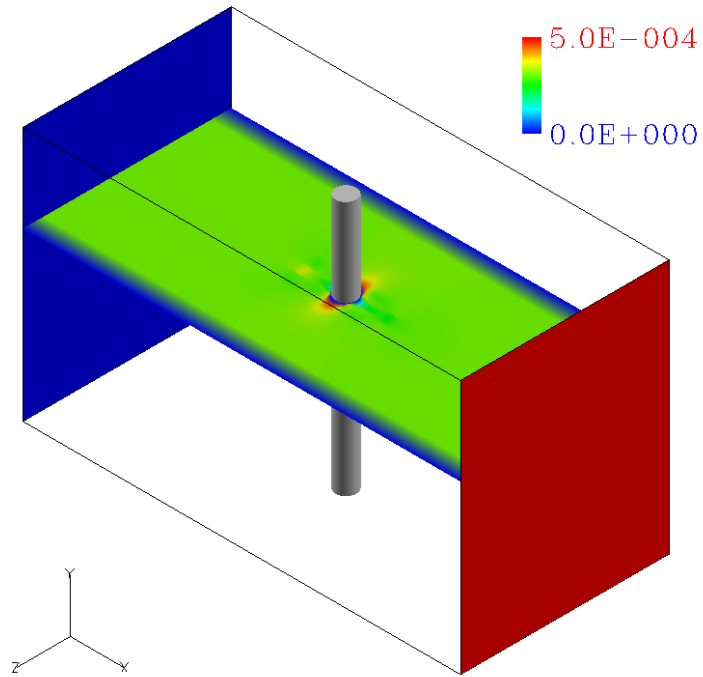
Figure 4.3. Isometric view of the velocity field (m/s) in the flow simulator around a 4-inch well with 4.0 gpm pumping rate. Flow is from left to right with inlet in blue and outlet in red.
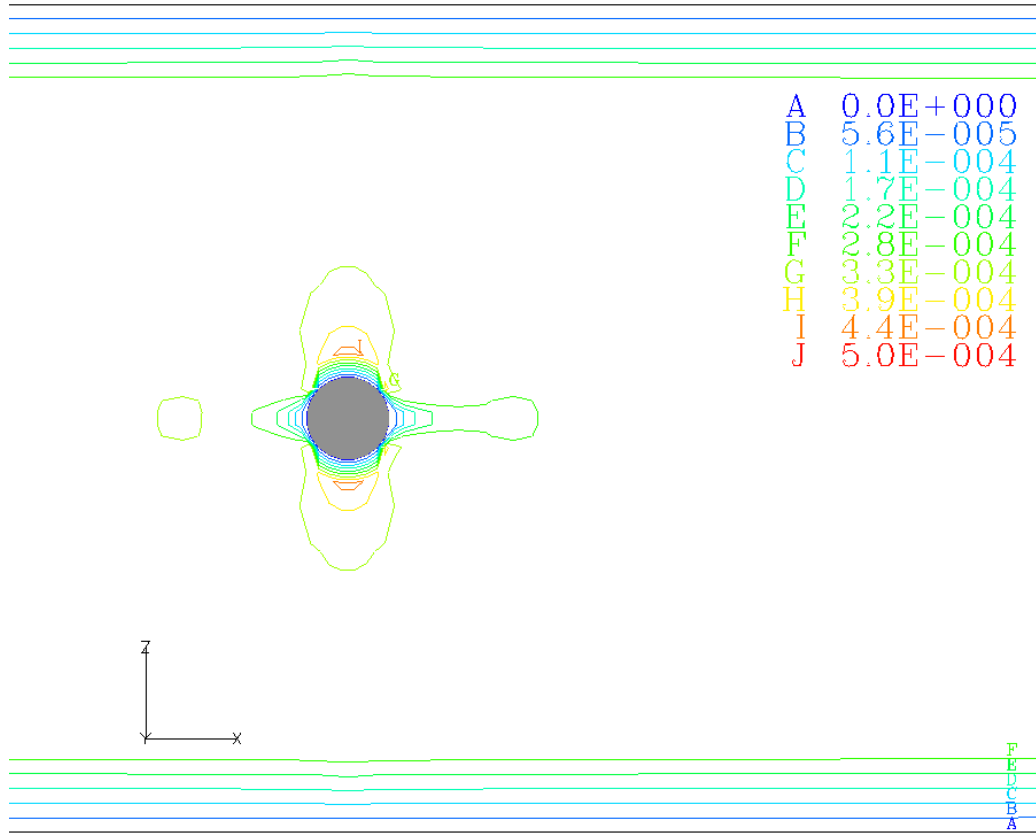
Figure 4.4. Top view of the velocity field (m/s) in the flow simulator around a 4-inch well with 4.0 gpm pumping rate. Flow is from left to right.

4.2 Inlet Velocity for Fractured Well in Flow Simulator

The model results from Section 4.1 show that the well does not affect the flow field beyond 15 cm from the well boundary. Therefore, the geometry was reduced to this size and the grid cells were significantly reduced for the computations involving the velocity of the inlet fracture in the well. The model for the reduced geometry and grid size is shown in Figure 4.5. Appendix 1 gives the grid cell number and spacing for the model. The grid used in the well interior has 16 cells in the x-direction in order to gain a fine resolution near the inlet. Since the fracture is 1.5 mm in the y-direction, only three cells were used in the fracture region (region 2).
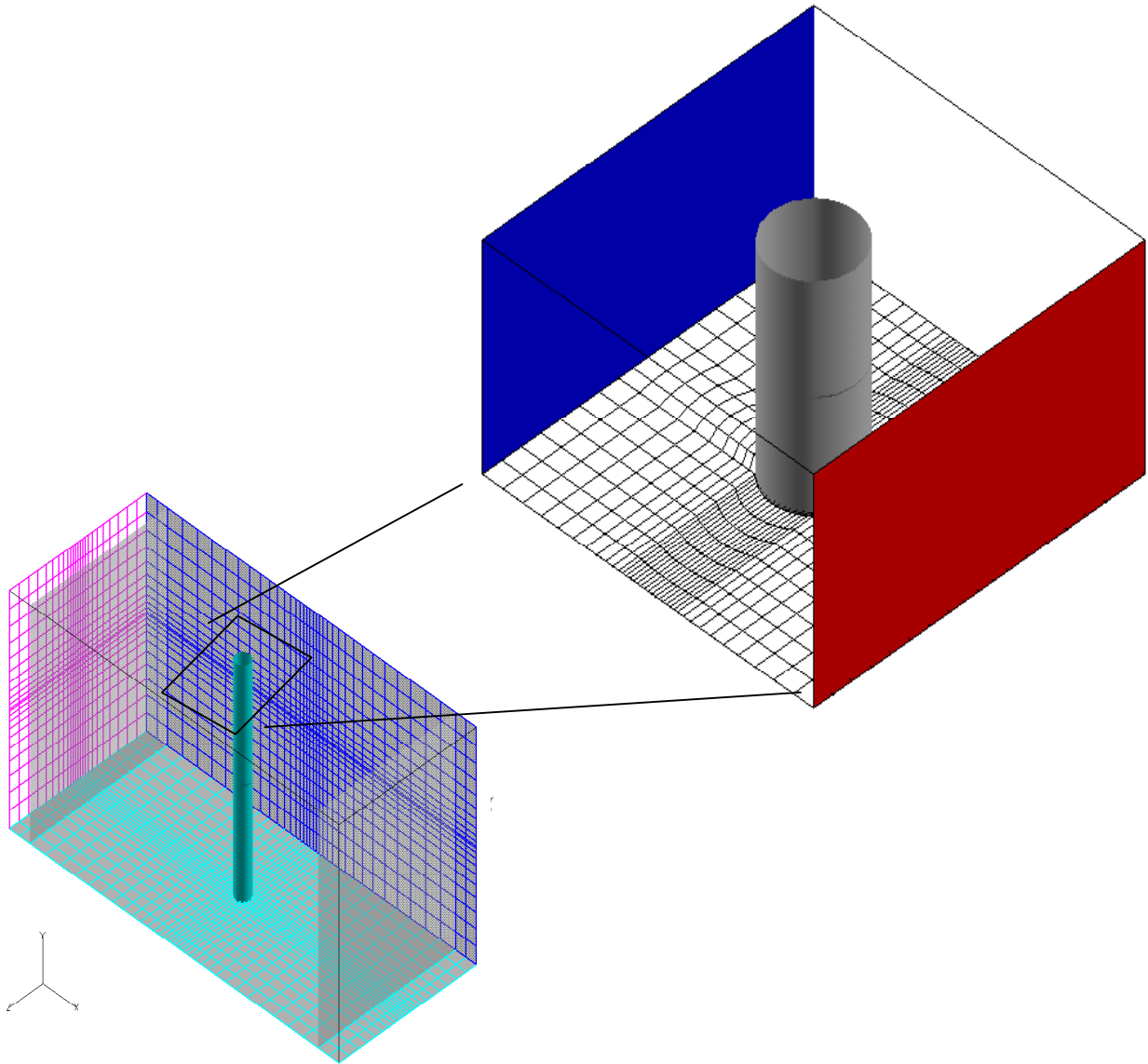
Figure 4.5. Isometric view of geometry and grid cells for reduced geometry. The inlet is blue and the outlet is red.
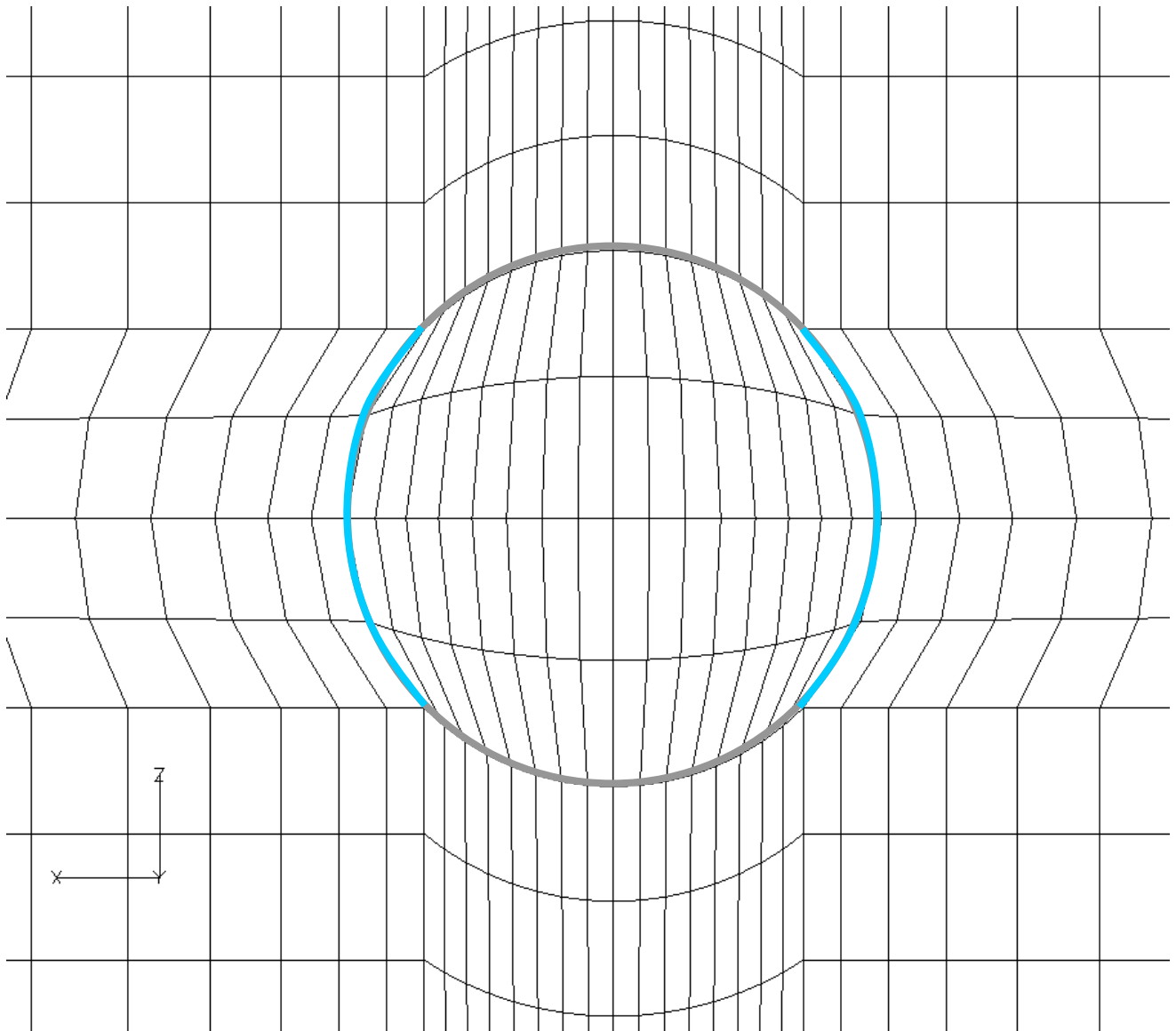
Figure 4.6. Zoomed in, top view of geometry and grid cells for reduced geometry. Grid cells used to determine inlet velocity are checked with an X. The thick gray line is the borehole wall and the blue line is for the fracture inlet/outlet. Flow is from left to right.

Results from the numerical model showed that flow was symmetric about the center of the well in the z-direction. Therefore, only four cells were monitored and recorded for the inlet velocity. Since the fractured well provides a preferential pathway with respect to the porous media, flow accelerates towards the fracture in the porous media near the well. Table 4.2 shows

the results for flow conditions in the porous media away from the effects of the fractured well and the increased velocity at the inlet for the range of flow rates used in the flow simulator.

Table 4.2. Flow through the porous media outside of the effects of the well and fracture inlet velocities for various pump rates.

Pump Rate (gpm)	Darcy Velocity (µm/s) (porous media)		Linear Advective Velocity[4] (µm/sec) (porous media)		Average Fracture Inlet Velocity (µm/s) for cells 10,19,8 / 10,10,9 / 11,10,8 / 11,10,9
	model	drawdown	model	drawdown	
0.4	3.1E+1	2.95E+0	8.99E+01	8.55E+0	2.1E+3
1.0	7.7E+1		2.23E+02		4.7E+3
1.3	1.15E+2	5.89E+0	3.33E+02	1.71E+1	7.0E+3
2.6	1.9E+2	1.06E+1	5.51E+02	3.07E+1	1.0E+4
4.0	3.1E+2	2.52E+2	8.99E+02	7.30E+2	1.65E+4

In addition, Figure 4.7 illustrates the effect of the preferential pathway through the fracture and the increased velocity at the inlet compared to that found far away from the fracture.

---

[4] Linear Advective Velocity = *Sd/porosity*
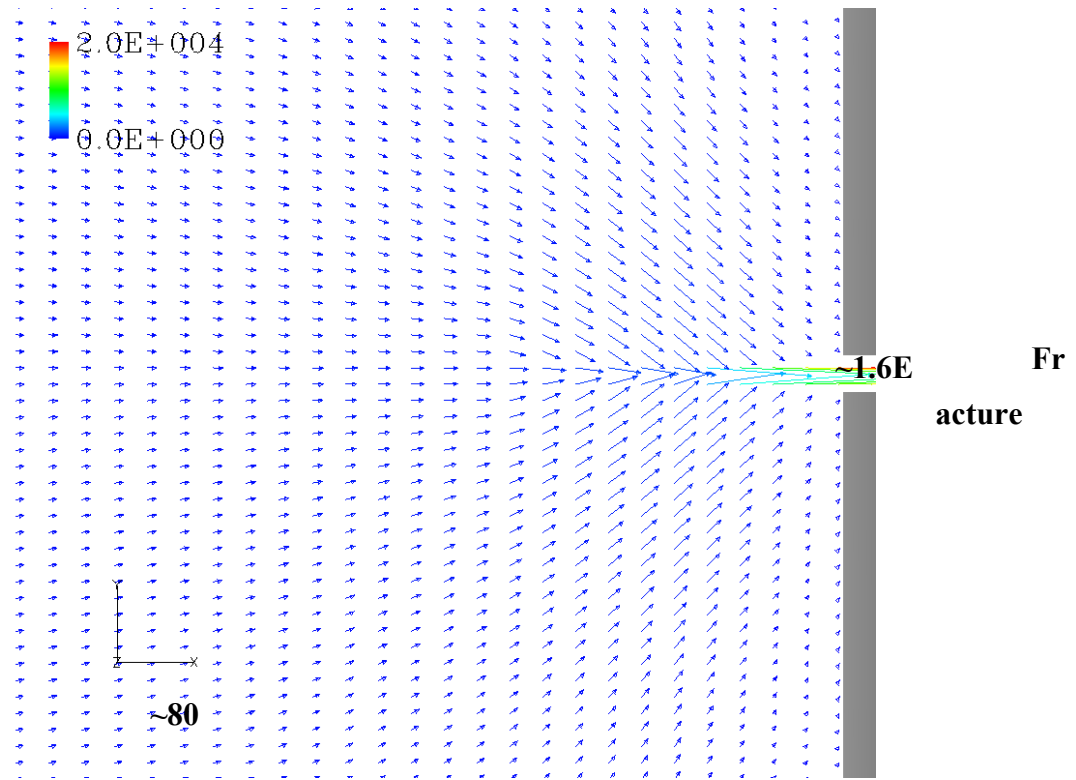
Figure 4.7. View of flow field near inlet of fractured well.

4.3 Scanning Colloidal Borescope Flow Meter (SCBFM) in Fractured Well

The inlet velocities calculated in Section 4.2 are the input for the inlet conditions of the model used for the interior of the well. This includes the Scanning Colloidal Borescope placed in the well such that the center of the viewing range of the borescope is located at the fracture horizon. The model geometry and grid spacing is shown in Figure 4.8.

S

nlet

]

ight
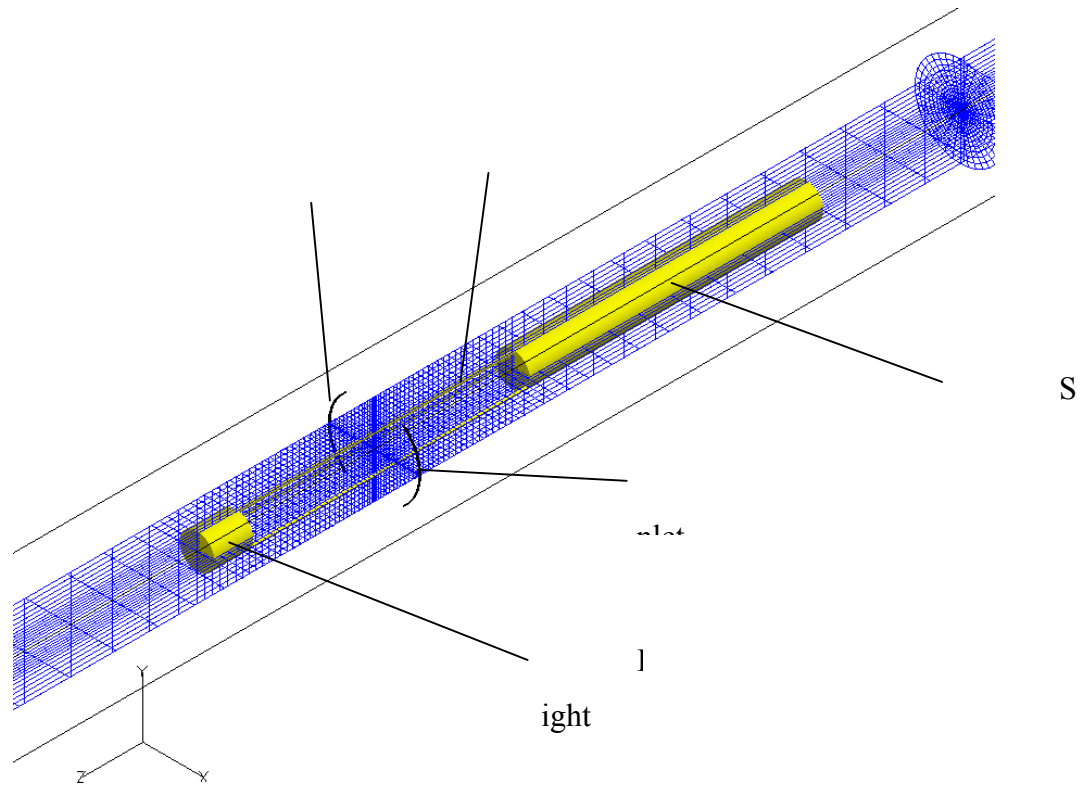
Figure 4.8. Isometric view of model geometry and grid cells for flow of the well interior with the SCBFM.

The geometry was created in cylindrical coordinates and a very fine grid was used in the region where the experimental tests by RAS were performed with the SCBFM. The grid cell number and spacing for the interior well model are given in Appendix 1, Table A2.

This model was run five times for each inlet condition calculated in Section 4.2. The results are shown in Figures 4.9 through 4.13. The results show that for the lowest flow rate (0.4 gpm), the inlet velocity dissipates quickly in the open hole and there is little effect of the velocity from the fracture inlet on the flow in the well. In the center of the well, where the SCBFM measures velocity and direction, the velocity is approximately 100 µm/s in the x-direction. This is more than two orders of magnitude slower than the velocity at the fracture inlet. However, at the highest flow rate (4.0 gpm), the effects of the fracture inlet pass well through the center of the well and the velocity in the center is approximately 5000 µm/s. This is only three times slower than the fracture inlet velocity. For the given conditions, the fracture inlet appears to have the

greatest impact on the center of the well at pump rates at or above 1.5 gpm in the flow simulator. Slower flow rates and associated inlet velocities dissipate in the open hole and their effects at the center of the hole are minimal.

In addition, the model shows that the scanning borescope itself is not interfering with the flow field. This can be seen in Figures 4.9 through 4.13 for the three-¼ inch light source attachments and in Figure 4.14 for the remainder of the borescope housing. Figure 4.14 shows that the flow from the fracture inlet dissipates into vertical circulation cells without reaching the housing for the borescope sensor (top) and light source (bottom). The tops of the circulation cells where the flow reverses direction across the center of the well are approximately 15 cm above and below the centerline. This would suggest that when the SCBFM is deployed in a real borehole in a fractured environment, the depth of the tool should be adjusted such that the flow interval of interest is kept 150 mm from the top and bottom of the scanned interval.
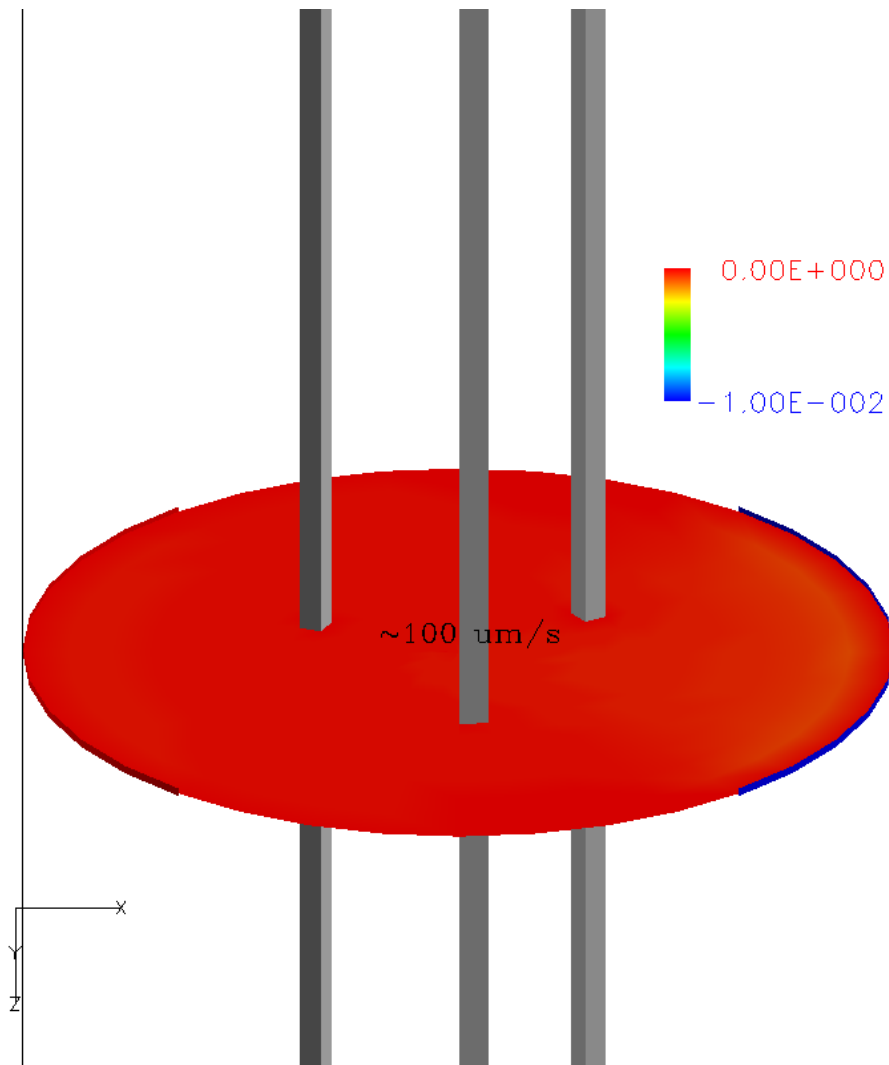
Figure 4.9. 0.4 gpm pump rate. Color scale is for velocity in the x-direction in m/s. The fracture inlet is on the right and flow is from right to left. Support rods (3) are shown through the center. The camera is above and the light source is below the fracture horizon.
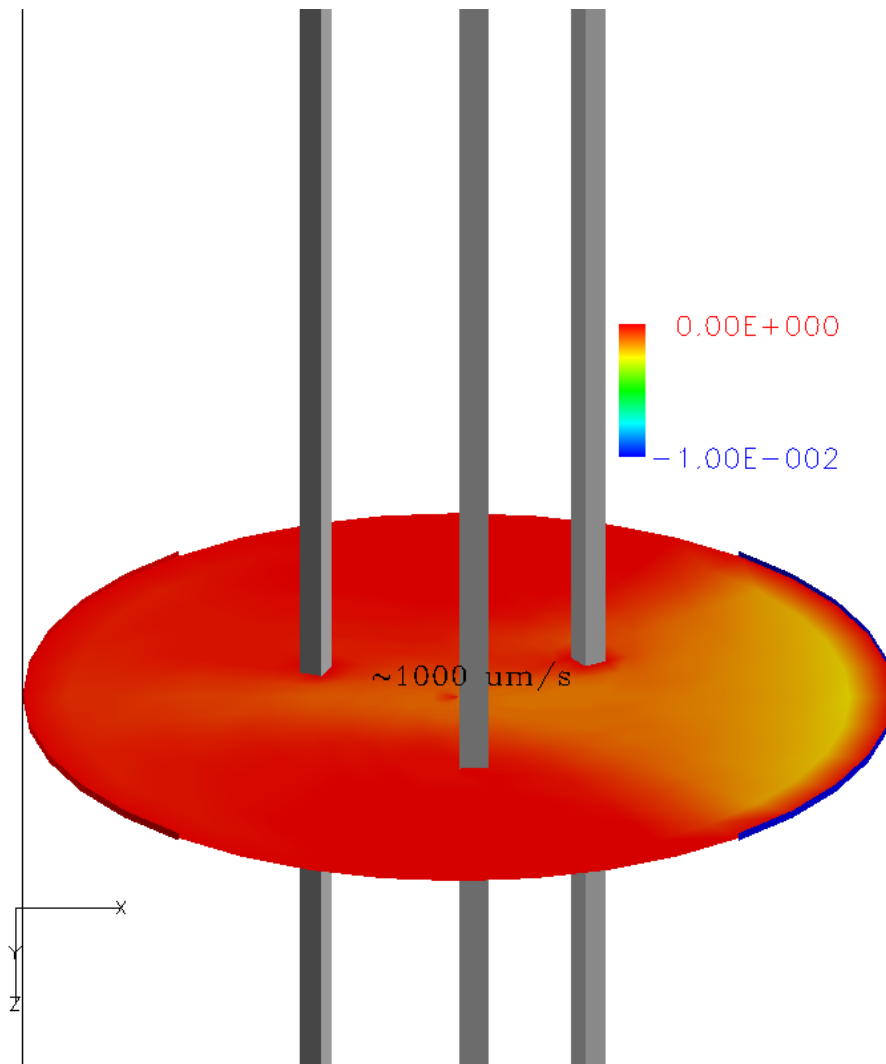
Figure 4.10. 1.0 gpm pump rate. Color scale is for velocity in the x-direction in m/s. The fracture inlet is on the right and flow is from right to left. Support rods (3) are shown through the center. The camera is above and the light source is below the fracture horizon.
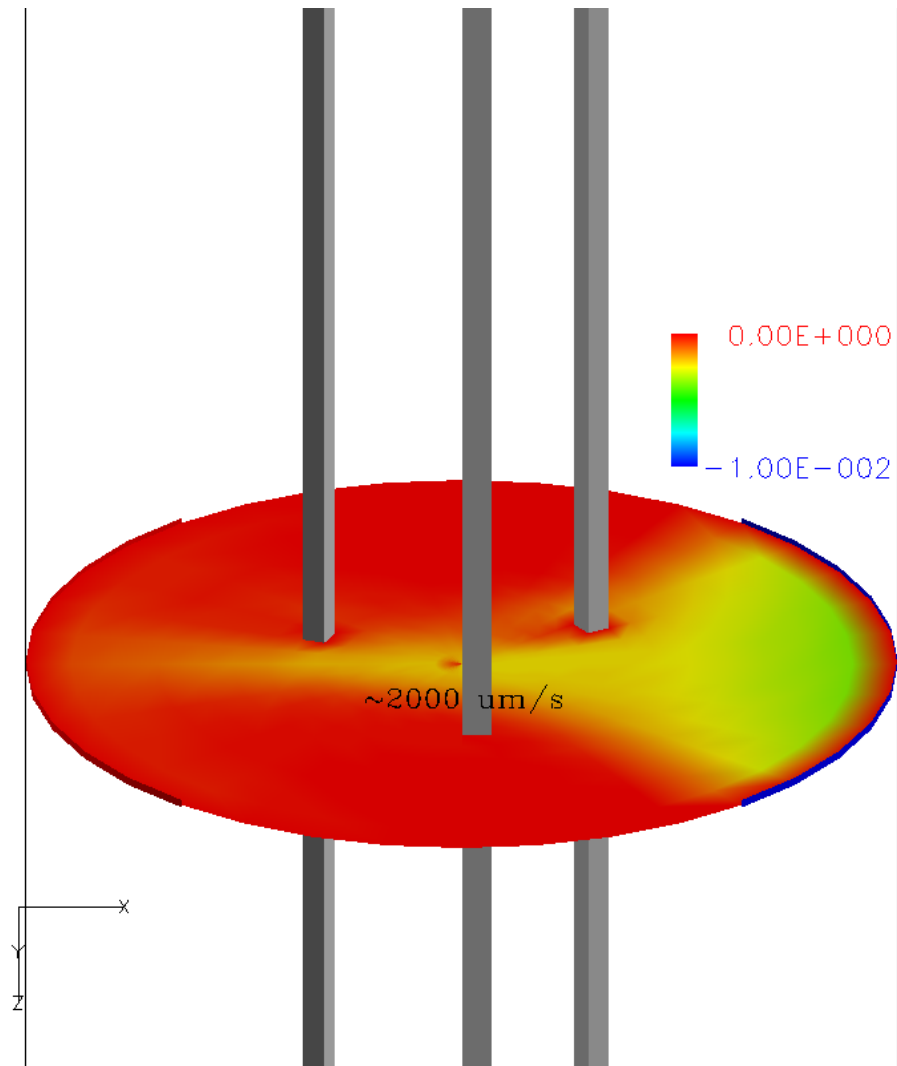
Figure 4.11. 1.5 gpm pump rate. The color scale is for velocity in the x-direction in m/s. The fracture inlet is on the right and flow is from right to left. Support rods (3) are shown through the center. The camera is above and light source is below the fracture horizon.
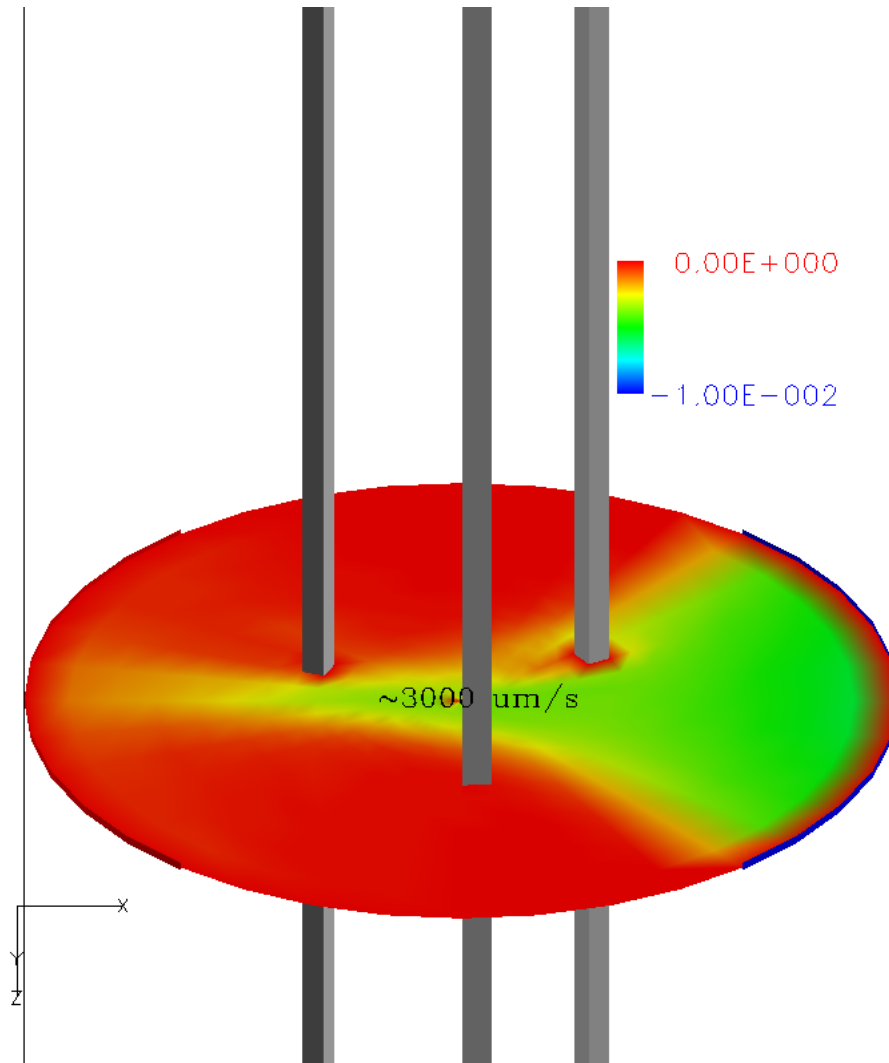
Figure 4.12. 2.5 gpm pump rate. The color scale is for velocity in the x-direction in m/s. The fracture inlet is on the right and flow is from right to left. Velocity depicted is for the center point and corresponding point of SCBFM measurement. Support rods (3) are shown through the center. The camera is above and light source is below the fracture horizon.
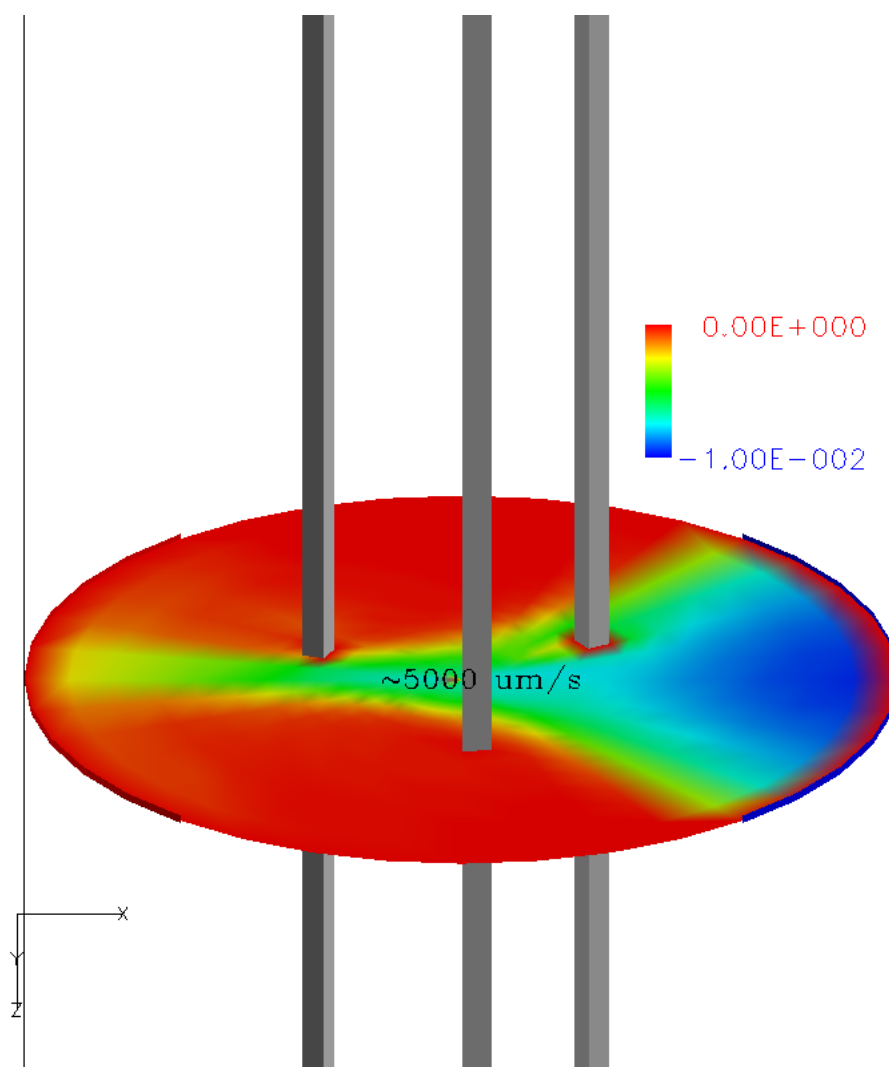
Figure 4.13. 4.0 gpm pump rate. The color scale is for velocity in the x-direction in m/s. The fracture inlet is on the right and flow is from right to left. Support rods (3) are shown through the center. The camera is above and the light source is below the fracture horizon.
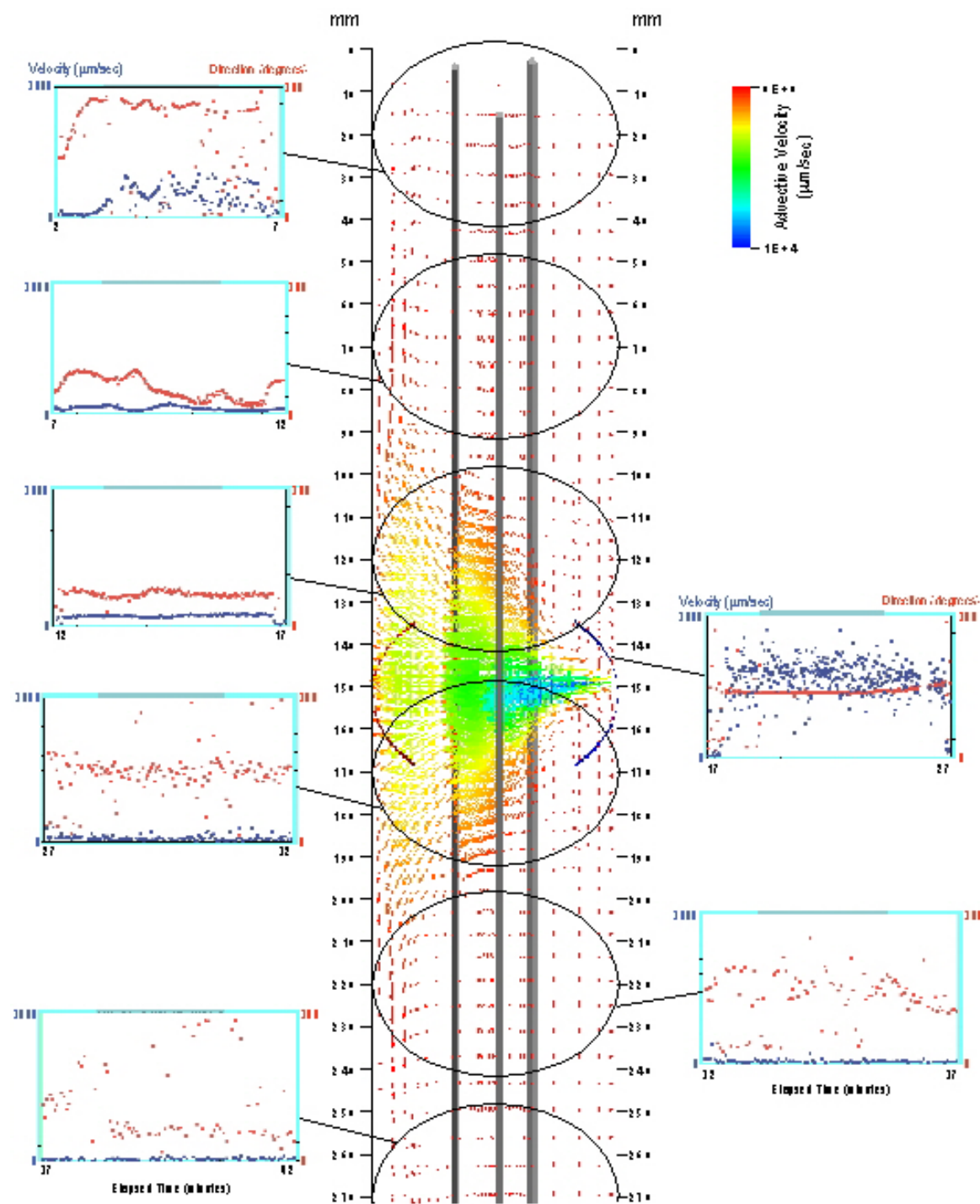
Figure 4.14. X-Z planar view tilted 30 degrees in the y-direction at 4.0 gpm pump rate. Color scale is for velocity in the x-direction in m/s. t and flow is from right to left.

4.4 Other Fracture Configurations

Two additional modeling tests were performed to investigate the width of the fracture. The fracture height of 1.5 mm was kept the same and the width was changed to 10 degrees and 180 degrees from the previous tests of 90 degrees. These configurations could be representative of a parallel plate model equivalent fracture (180 degrees) and a channel-type equivalent fracture (10 degrees). Results are shown in Figure 4.15 for an inlet velocity of 2E-3 m/s. Results show that the velocity at the center is similar for the 180 and 90-degree case. However, for the 10-degree case, the effects of the inlet are very local to the location of the fracture. A significant inlet velocity would have to be used to generate a velocity at the well center for the 10-degree fracture width.
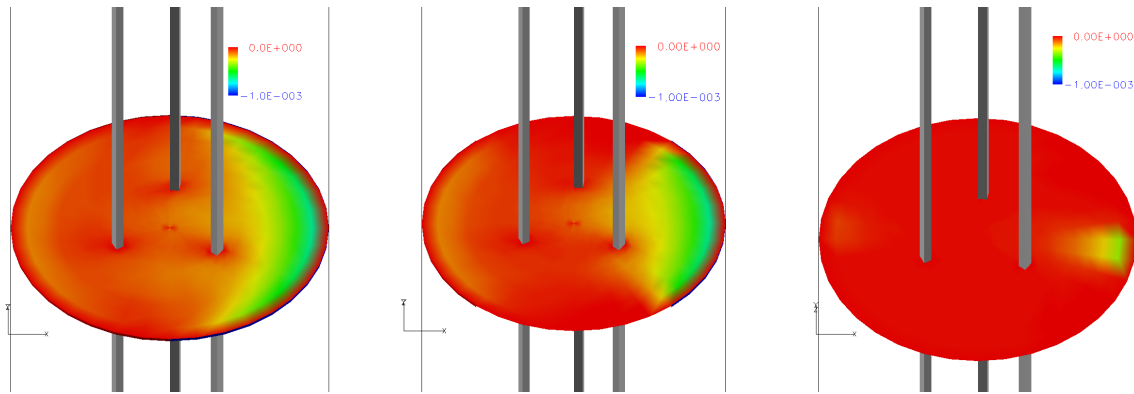
Figure 4.15. Model results for 180, 90, and 10-degree fracture widths. Color scale is for velocity (m/s) in the x-direction. *Note the color scale is different from that shown in Figures 4.9-14.*

5.0 Comparisons of Model and Experimental Results

Both the Hydrophysics and Scanning Colloidal Borescope measurements allow for comparisons to modeling results. The hydrophysics comparison is primarily for the results regarding the fracture velocity and the SCBFM comparison is for the velocity at the center of the well.

5.1 Fracture Inlet Velocity

The hydrophysical measurements allow for an estimate of the total flow rate through the well. Since the flow in and out of the well was confined to the 1.5 mm inlet and outlet fractures, a velocity at the fracture could be calculated (Section 3.2). The model calculated an inlet velocity from the method described in Section 4.2. A comparison of the experimental and modeling results is shown in Table 5.1.

Table 5.1. Comparison of model and experimental results for inlet fracture velocity.

Flow Rate Across Simulator (gpm)	Hydrophysics Measurement from Integral Analysis (μm/s)	Model Result (μm/s)
0.4	1590	2100
1.3	2647	6100
2.5	4235	10000
4.0	5294	16500

The model results match closely at the low flow rate but are higher by a factor of 2 to 3 for the larger flow rates.

5.2 Velocity at the Center of the Well

The Scanning Colloidal Borescope directly measures the velocity of the colloidal particles at the center of the well. The model described in Section 4.3 specifically calculates the conditions in the interior of the well based on a given inlet fracture velocity. Table 5.2 compares

the results for the model near the center of the well with that measured by the Scanning Colloidal Borescope.

Table 5.2. Comparison of model and experimental results for velocity at the center of the well.

Flow Rate Across Simulator (gpm)	Borescope Measurement (μm/s)	Model Result (μm/s)
0	2	0
0.4	55	~100
1.0	110	~1000
1.5	-	~2000
2.5	1600	~3000
4.0	-	~5000

Again, the model results give larger values by about a factor of two. This is similar to the results for the fracture velocity.

The experiments also indicated that the flow through the center of the well was a very narrow jet. Visual observation of the colloids from the SCBFM demonstrated that the particles would travel faster on one side of the viewing area compared to the other side. (Please see the video tape which accompanies this report.) This observation is consistent with the model results shown in Figures 4.9-4.13 in which a narrow jet through the center is clearly visible at the higher flow rates.

In addition, the scanning option on the SCBFM was used to investigate the flow field above and below the fracture at the higher flow rates (>2 gpm). Visual observation noted virtually no flow immediately (>1 cm) above and below the fracture horizon. At distances approximately 10 to 15 cm above and below the fracture horizon, flow of a lesser magnitude was observed in the opposite direction compared to that at the fracture. This indicated the outer limit of a circulation cell within the well caused by the relatively high flow velocity entering the well at the fracture inlet. Figure 4.14 also shows a circulation cell where the extent of the circulation is 15 cm above and below the fracture horizon.

6.0 Conclusions

The results of this work show that: 1) the flow simulator is an excellent method for testing the Scanning Colloidal Borescope Flow Meter (SCBFM) and Hydrophysical tools under known, controlled conditions; 2) the measurements made by the two experimental tools are in good agreement at all flow rates tested; and, 3) the model is capable of predicting flow conditions in the simulator and interior of the well. The properties and flow rates used in the simulator provide a wide range of conditions in the well that are similar to those observed in field tests. The model predicted qualitatively similar results with regard to the observed flow characteristics in the well. This was noted by the prediction of the jet through the center of the well and the circulation cells above and below the fracture horizon. However, the model over-predicted both the fracture inlet velocity and velocity across the center of the well by about a factor of two. Nonetheless, it is very encouraging that the model is consistently higher by the same factor. It appears that the origin of the difference between the model and the measurements is the calculation of the inlet fracture velocity. A modification of the model used to calculate the inlet velocity could be done to: 1) create a higher grid resolution near the fracture; or, 2) create a geometry such that the grid cell center is at the edge of the well rather than using the cell immediately inside and outside the well. If the inlet velocity as predicted by the model were reduced by a factor of two, the subsequent calculation of the center velocity in the well would likewise be reduced by the same multiple.

The preliminary conclusions of this work suggest the following; 1) horizontal flow in the fractured medium which is representative of the near field flow conditions can be established in a wellbore; 2) that this horizontal flow can be accurately measured and numerically predicted; 3) that the establishment of directionally quantifiable horizontal flow is dependent on four parameters: borehole diameter, structure, permeability and the hydraulic gradient of the flowing feature; and, 4) by measuring three of these four parameters, the fourth parameter can be numerically derived through computer simulations.

In summary, the results for the design, construction, and testing of the flow simulator along with the creation of the numerical models were very successful. Future work could focus on making small improvements with regard to the model grid and geometry for the calculation of the inlet velocity. Once this is accomplished and tested, further investigations of various fracture

configurations in the flow simulator could be done. The model could be used to guide decisions on fracture configurations that would provide the most useful information. This would lead to a much-improved understanding of the benefits and limitations of the tools used to measure properties in the borehole and relating them to the subsurface media.

7.0 References

Bear, J., D. Zaslavsky, and S. Irmay, 1968. *Physical Principals of Water Percolation and Seepage*, UNESCO, Paris, 465pp.

BIBLIOGRAPHY FOR HYDROPHYSICAL LOGGING

Anderson, W.P., D.G. Evans, and W.H. Pedler, 1993. "Inferring Horizontal Flow in Fractures Using Borehole Fluid Electrical Conductivity Logs," EOS, Transactions of the American Geophysical Union Fall Meeting Vol. 74, No. 43, pg. 305, Dec. 1993.

Beauheim, R.L., L.C. Meigs, and M.B. Kloska. 1995. "Evaluation of Conceptual Models of Flow and Transport Through a Fractured Dolomite: 1. Hydraulic Testing," Presented at the 1995 AGU Fall Meeting, San Francisco, CA, Dec. 11-15, 1995; abstract in Eos, Transactions, American Geophysical Union. Vol. 76, no. 46, F251.

Beauheim, R.L., L.C. Meigs, and P.B. Davies. 1997. "Rationale for the H-19 and H-11 Tracer Tests at the WIPP Site," OECD Documents, Field Tracer Transport Experiments, Proceedings of the First GEOTRAP Workshop, Cologne, Germany, 28-30 August 1996. Paris, France: OECD NEA.

Crowder, R.E., and W. H. Pedler, 1993. "Integration of Borehole Geophysical and Fluid Logging Methods for Fractured Bedrock Characterization," EOS, Transactions of the American Geophysical Union Fall Meeting Vol. 74, No. 43, pg. 567, Dec. 1993.

Doe, T. and W.H. Pedler, 1998, The Problem of Fractures, Ground Water Monitoring and Remediation, Winter 1998, pages 74-77.

Evans, D.G., Anderson, W.P., and Tsang, C.F., "Borehole Fluid Experiments Near Salt Contamination Sites in Maine," Research Project conducted under U.S. Department of Energy, Environmental Restoration and Waste Management Young Faculty Award Program, 1992.

Evans, D.G., "Ordinary and Constrained Least Squares Inversion of Borehole Fluid Logs," EOS, Transactions of the American Geophysical Union Fall Meeting Vol. 74, No. 43, pg. 305, Dec. 1993.

Evans, David G. Inverting Fluid Conductivity Logs for Fracture Inflow Parameters, to appear in Water Resour. Res., 1995 (in press).

Evans, David G. and Gerald Janowitz, Determining groundwater velocities from borehole dilution experiments with diffusion in the wellbore, submitted to Water Resour. Res., Aug. 1995 (in revision).

Evans, D.G., C.B. Lane, F. Paillet and W.H. Pedler, Hydraulic characterization of fractures in the Piedmont of North Carolina using fluid conductivity and transient flow logging, Geol. Soc. Am. Programs and Abstracts, Southeastern Regional Meeting (1996).

Hale, F.V. and Tsang, C.F., "A Code to Compute Borehole Fluid Conductivity Profiles with Multiple Feed Points," LBL-24928, Lawrence Berkeley Laboratory, University of California, Berkeley, CA and NDC-8, NAGRA-DOE Cooperative Project, and NTB 88-21, Nagra, Baden, Switzerland, March 1988.

Kelley, V.A., Loew, S., Vorvormis, E., "Determination of Fracture Connections in a Granite from a Pilot Crosshole Fluid Logging Test", EOS, Transactions of the American Geophysical Union Fall Meeting, Vol. 72, No. 44, pg. 216, Dec. 1991.

Lane, Craig, Comparison of Hydrophysical Logging to Other Borehole Testing Techniques to Characterize Hydraulic Properties of Bedrock Fractures, Raleigh, North Carolina. MS Thesis, Department of Marine, Earth and Atmospheric Sciences, North Carolina State University (1995).

Loew, S., Ehlers, F., Andrews, R., McNeish, J., Vomvoris, and Hufschmied, P., "Quantitative Analysis of Electrical Conductivity Logs in the Leuggern Borehole (Switzerland)," Transactions of 1988 American Geophysical Union, Vol. 69, No. 44, pg. 1172, 1988.

Loew, S. (Nagra), C.F.Tsang, F.V. Hale and P. Hufschmied (Nagra), "The application of moment methods to the analysis of fluid electrical conductivity logs in boreholes," LBL-28809, Lawrence Berkeley Laboratory, University of California, Berkeley, CA, and NDC-8, NAGRA-DOE Cooperative Project, Nagra, Baden, Switzerland, August 1990.

Long, J.C.S., E.L. Majer, K.Karaski, C.L. Carnahan, J.S. Jacobsen, K. Hestir, D. Billaux, J. Peterson, L.R. Myer, and C.F. Tsang, "The NAGRA-DOE cooperative research program," pp. 185-188, in Earth Sciences Division Annual Report 1987, LBL-24200, UC-403, Lawrence Berkeley Laboratory, University of California, Berkeley, CA, September 1988.

Paillet, F.L, Kay, R.Y., Yeskis, D, and Pedler, W.H, "Integrating Well Logs into a Multi-Scale Investigation of a Fractured Sedimentary Aquifer", *The Log Analyst*, pgs. 24-41, Jan.-Feb., 1993.

Paillet, F.L. and Pedler, W.H., Integrated Borehole Logging Methods for Wellhead Protection Applications, Engineering Geology 42 (1996) pages, 155-165, reprints available through Elsevier Science Publishers.

Pedler, W.H., and Urish, D.W., "Detection and Characterization of Hydraulically Conductive Fractures in a Borehole: The Emplacement Method," EOS, Transactions of the American Geophysical Union Fall Meeting Vol. 69, No. 44, pg. 1186, Dec. 1988.

Pedler, W.H., Barvenik, M., Gardner, G., and Urish, D.W., "Detection and Characterization of Hydraulically Conductive Fractures by Geophysical Logging after Fluid Emplacement," Proceedings of the Second Annual Hazardous Materials Management Conference/Central, pgs. 121-129, 1989.

Pedler, W.H., Barvenik, M.J., Tsang, C.F., Hale,F.V., "Determination of Bedrock Hydraulic Conductivity and Hydrochemistry Using a Wellbore Fluid Logging Method," Proceedings of the Fourth National Water Well Association's Outdoor Action Conference, Las Vegas, NV, May 14-17, 1990; reprint LBL-30713, Lawrence Berkeley Laboratory, University of California, Berkeley, CA.

Pedler, W.H., and Kennard, M., "Hydrophysical Logging: An Advanced Wellbore Technology for Hydrogeologic and Contaminant Characterization of Aquifers," Proceedings of the 1992 Joint Meeting of the Arizona Hydrological Society/ Commission on the Arizona Environment, Arizona Water 2000.

Pedler, W.H., Tsang C.F., and Hale, F.V., "A Wellbore Fluid Logging Method for Characterizing Bedrock Aquifers," pp. 64-66 in Earth Sciences Division Annual Report 1990, LBL 27900, UC-403, Lawrence Berkeley Laboratory, University of California, Berkeley, CA, June 1991.

Pedler, W.H., "A Wellbore Fluid Logging Method for Aquifer Characterization," EOS, Transactions of the American Geophysical Union Fall Meeting, Vol. 72, No. 44, pg. 216, December 1991.

Pedler, W.H., Head, C.L. and Williams, L.L., "Hydrophysical Logging: A New Wellbore Technology for Hydrogeologic and Contaminant Characterization of Aquifers," Proceedings of Sixth National Outdoor Action Conference, National Groundwater Association, May 11-13, 1992.

Pedler, W.H., "Evaluation of Interval Specific Flow and Pore Water Hydrochemistry in a High Yield Alluvial Production Well by the Hydrophysical Fluid Logging Method" EOS, Transactions of the American Geophysical Union Fall Meeting Vol. 74, No. 43, pg. 304, Dec. 1993.

Pedler, W.H., "Integrated Borehole Logging Methods for Wellhead Protection," Proceedings of the 36th Annual Association of Engineering Geologist Meeting, page 66, 1993.

Pedler, W.H., Kennard, M., "Hydrophysical Logging at the WQARF Site; Payson, Arizona," Proceedings of the Arizona Hydrological Society Sixth Annual Symposium, 1993

Pedler, 1997, Hydrophysical Logging: A Review of Applications and Case Studies, Proceedings of Joint Russian-American Hydrogeology Seminar, Lawerence Berkeley National Laboratory, July 8-9, 1997, LBNL publication PUB-804, pages 275 – 302.

Pedler, W.H. and L.L. Williams, 1998, Collecting Legally Defensible Subsurface Data for Use in Litigation, Environmental Compliance and Litigation Strategy, March 1998, pages 6 - 7.

Tsang, C.F. and P. Hufschmied, "A Borehole Fluid Conductivity Logging Method for Determination of Fracture Inflow Parameters," LBL-23096, Lawrence Berkeley Laboratory, University of California, Berkeley, CA October 1987, NDC-1, NAGRA-DOE Cooperative Project and NTB-88-13, NAGRA, Baden, Switzerland, January 1988. Note that this report has been superseded by Tsang, Hufschmied and Hale, 1989.

Tsang, C.F., F.V. Hale, and P. Hufschmied, "Determination of Fracture Inflow Parameters with a Borehole Fluid Conductivity Logging Method," Water Resources Research, vol. 26, no.4, pp. 561-578, April 1990 and LBL 24752, Lawrence Berkeley Laboratory, University of California, Berkeley, CA, and NDC-1, NAGRA, Baden, Switzerland, September 1989.

Tsang, C.F. and F.V. Hale, "A Direct Integral Method for the Analysis of Borehole Fluid Electrical Conductivity Logs to Determine Fracture Inflow Parameters," pp. 108-110 in Earth Sciences Division Annual Report 1988, LBL-26362, UC-403, Lawrence Berkeley Laboratory, University of California, Berkeley, CA, August 1989.

Tsang, C.F. and F.V. Hale, "A Direct Integral Method for the Analysis of Borehole Fluid Conductivity Logs to Determine Fracture Inflow Parameters," in Proceedings, New Field Techniques for Quantifying the Physical and Chemical Properties of Heterogeneous Aquifers Conference, Dallas, Texas, March 20-23, 1989, F.J. Molz, ed., National Water Well Association, Dublin, OH.

Tsang, C.F., F.V. Hale, and P. Hufschmied, "Validation of a Method for Analyzing Borehole Fluid Conductivity Logs to Determine Fracture Inflow Parameters," pp/95-98 in Earth Sciences Division Annual Report 1989, LBL 27900, UC-403, Lawrence Berkeley Laboratory, University of California, Berkeley, CA June 1990.

Vernon, J.H, Paillet, F.L., Pedler, W.H., Moore, B.A., and Griswold, W.J., "Fracture Flow Assessment for Wellhead Protection Monitoring" *Groundwater,* in press, early 1996.

Vernon, J.H, Pedler, W.H., and Paillet, F.L., "Selected Borehole Geophysical Techniques for Well Protection in a Fractured Bedrock Aquifer", Special Environmental Edition, *The Log Analyst*, p. 41-58, Jan-Feb, 1993.

SCANNING COLLOIDAL BOREHOLE FLOW METER REFERENCES

Wood, W.K., Ferry R.F., and Landgraf, R.K., Direct Ground Water Flow Direction and Velocity Measurements Using the Variable-Focus (Scanning) Colloidal Borescope at Sandia National Laboratory, 1997, Lawrence Livermore National Laboratory Report, UCRL-AR-126781.

APPENDIX 1

Grid for CFD Models

Grid for determining inlet velocities from porous media to well fracture:

Table A.1. Grid cell number for each axis. Value in () for power of grid stretching.

Region	X	Y	Z
1	10 (1.4)	8	7
2	16	3	4
3	10 (1.4)	8	7

The grid generated for the model does not have a grid center at the inlet. In order to determine the velocity at the inlet of the fracture, the grid cells immediately outside the fracture and inside the well were monitored and averaged once they converged. Figure 4.6 shows the grid cells near the well and the cells that were used to determine the inlet velocity.

Grid for interior of borehole with SCBFM placed inside:

Table A.2. Grid cell number for each axis. Value in () for power of grid stretching.

Region	I	J	K
1	36	2	7
2	-	5	10 (1.4)
3	-	7 (1.2)	60 (1.5)
4	-	-	5
5	-	-	7 (1.4)

The 1.5 mm fracture horizon was chosen at the center of region 3 in the geometry or cell numbers 5 through 14 (I) for the inlet and 23 through 32 (I) for the outlet; 14 (J); and 47 (K) and covered a 90-degree span for both the inlet and outlet.

Distribution